Scattering phenomenon in Piton de la Fournaise volcano, Reunion island

Molina Aguilera, Antonio Manuel

1 Motivation

Interpreting the seismic signals in volcanic environments presents some difficult challenges in seismology. Several potential source mechanisms are thought to generate seismicity on active and/or restless volcanoes such as brittle rock failure, fluid transport, gas slug ascent, choked flow, magmatic activity and the interaction of hot magma with hydrothermal fluids (see Chouet (2003), McNutt (2005) for reviews of volcano seismology). This richness in the potential source mechanism is mirrored in the variety of classes of signals observed in volcanoes which span from ultra/long period events (100 s dominate periods) through very-long period events to long-period events and in addition volcano-tecnotic signals (McNutt, 2005). On the other hand, the complexity arises as well in volcanic setting because (1) the wavefield is significantly distorted by the complex topography, (2) the volcanic stratigraphy can further distort the wavefield and (3) the presence of magmatic fluids may generate large intrinsic attenuation. Adding to this complexity, as quite often the near-field seismic wavefield cannot be ignored, P- and S-wave phases can be intertwined. The combination of these processes can lead to a diffusive wavefield and the signals may have emergent wave-trains due to both source and path effects. Thus, a key question in volcano seismology is what are the relative effects of topography, structure and attenuation on the wavefield and how are they quantifiable?.

It is well known that these complexities in the volcanic environment make it difficult to obtain a stable source mechanism (Bean et al., 2008), inversions have been succesfully performed by several authors (Ohminato et al., 1998, Kumagai et al., 2002, Zecevic et al., 2013) but since the accuracy of the inversion strongly depends upon the Green's functions, uncertanties and errors in the velocity model (note that volcanoes often have a shallow, low velocity layer) and topography lead to erroneous source positions and mechanisms in the moment tensor inversion (Bean et al., 2008, O'Brien et al., 2010). Studies have so far concentrated on periods larger than 1 s (Davi et al., 2010), as seismic waves with long wavelength are less affected by small scale-heterogeneities (Ohminato et al., 1998, Bean et al., 2008). The simulation of a complete, higly accurate wave field at high frequencies may involve including high-resolution topography and small scale-heterogeneities in the numerical model, but the computational cost of building up meshes which honour properly the complex topography and, on the other hand, the poor knowledge of the internal volcanic structure, make it still a great challenge in volcanic seismology.

In the last years a new flexible and powerful simulation method has been developed that combines the Discontinuous Galerkin (DG) Method with a time integration method using Arbitrary high order DERivatives (ADER) of the aproximation polynomials (Käser and Dumbser, 2006, Käser et al., 2007, 2010, Etienne et al., 2010). The unique property of this numerical scheme is, that it achieves arbitrarily high approximation order for the solution of the governing wave equation in space and time on unstructured tetrahedral meshes which are well suited to model complex topography. Moreover, techniques for automatic mesh generation, gradual mesh refinement and coarsening are generally much more robust for tetrahedral in comparison to hexahedral meshes, factor that plays a crucial role when we must address complex geometries.

Therefore, the long-term aim of this work is to create the basis of a powerful seismic simulation tool making use of the developement of the ADER-DG algorithm and implementing as well an efficient and highly accurate mesh generation workflow. Moreover, these meshes might be available for the scientific community

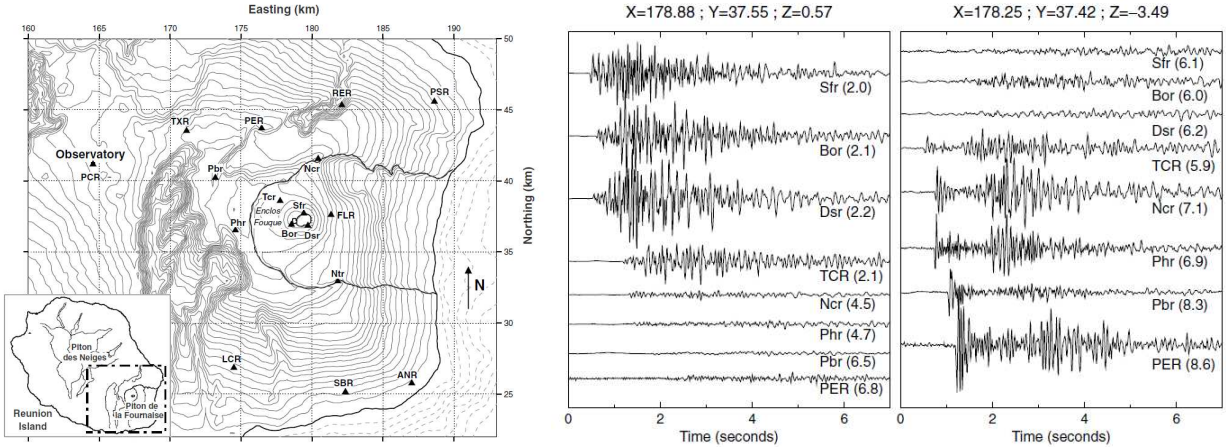

Fig. 1: Left: Map of the eastern part of Reunion Island with the seismic stations of the monitoring network (1998) represented as triangles. Geographical coordinates are Gauss-Laborde kilometric coordinates (transverse Mercator) and isolines are spaced every 200 m. Right: Comparison of waveforms recorded for an event located above sea level (left), below the summit, and those for an event recorded at 4.5 km depth (right). Waveforms are presented with a common vertical scale, after correcting for instrument magnification and recording site effects. The locations of the hypocentres are given in the upper part of each plot. The distance between the hypocentre and each station is given beside the name of the station (Battaglia et al., 2005).

through the VERCE project (www.verce.eu) which plans to stablish a community mesh-database to provide easy upload of and access to already created meshes for and by the users.

As a first application, Piton de la Fournaise volcano (La Reunion island), one of the most active volcanoes in the world, stands as a propitious scenario: there is a high resolution digital elevation model (5 m resolution), a seismic network consisted of 21 three component broadband stations with a good coverage on the summit (UnderVolc project), and a relative deep knowledge of its inner structure since it has been extensively studied and monitored for several decades. In addition to this, a very local path effect seems to take place in some stations located close to the summit of the volcano. Modeling this phenomenon encourages us to start implementing our workflow using Piton de la Fournaise volcano.

Thought it is still quite unknown the scattering mechanism that produces the local effect on the volcano, Battaglia et al. (2005) have slightly discussed it. According to them the stations affected are located quite close to the summit of the volcano and just for those events whose depth is larger than 1 km bsl. They compare the waveforms of a shallow earthquake (above sea level) with another one whose hypocentre is below a high-seismicity zone (3.5 km bsl) (see Fig. 1). While for the shallow event the amplitude of the waveforms decays proportionally to the distance to the source, for the deeper one amplitudes are larger at stations situated away from the summit (see PER, Pbr, Phr or Ncr), the waveforms at the summit stations (Sfr, Bor and Dsr) situated closer, are attenuated. Battlagia et al. suggest the presence of a zone of high attenuation for seismic waves bsl which is related to a high-seismicity zone and mostly affecting earthquakes deeper than 1 km bsl.

In order to illustrate roughly this propagation path effect we show at first a very extreme case for a volcanotectonic earthquake whose source depth is 11 km bsl. —> Show the location of this event?????. 2 depicts the 3-component seismograms and spectrograms (E, N and Z from left to right) for the stations located nearby the summit (each trace has been normalized by its maximum amplitude to compare easily the waveforms). The seismic signal for the stations no located on the summit is characterized by an impulsive onset clearly visible, especially in the vertical component, and a relatively high frequency content (ranging from 5 to 30 Hz) with a short bandwith of a few seconds (about 3 s). The impressive characteristic of the

seismograms located quite close to the summit (stations shown colored in red: UV11, UV15, UV05 and SNE) is their envelopes. The strongest amplitudes in the recordings are not caused by the direct P- and S-wave arrivals but the main part of the energy is shifted to the later times in the seismogram. Following the first onset, which has a very small amplitude (in this case the small P onset is already below the noise level and it can not be distinguished), the energy slowly and continuously increases to a maximum value in the way of an emergent wave train. The late part of the seismogram following the energy maximum can be described by an exponential decay. Althought this difference in the signal can be observed in the three components is more distinguishable in the Z channel since the P onset is often clearer in the vertical component. On the other hand, the frequency content of the signal also changes dramatically for the stations located on the summit, the dominant frequencies are concentrated in lower values and the signal shows a more distributed over time frequency content (for some stations such as UV05 the very low signal-to-noise ratio results in a spectrogram which basically plots noise). We point out that the source-receiver distances for the stations selected in 2 are very similar due to the large depth of the seismic event as it is shown on the right of the seismic E component trace. -> Prepare a figure of the seismic network used in this study and mention here the distance.

Therefore, this dramatic difference in the wavefield among the stations located on Piton de la Fournaise seems to be a clear example of a very local propagation path effect. Our purpose is, primarily, characterize the phenomenon (1) looking for those seismic observables that best highlight the mentioned behaviour and (2) elucidating which possible scattering mechanisms may produce it. After that, we devise a viable strategy to model the phenomenon for high frequencies with the still in developing workflow.

2 Some previous information of PdF

Piton de la Fournaise is a basaltic, shield volcano located in the south-east of la Réunion Island in the Indian Ocean, about 800 km east of Madagascar (see figure 3). It is associated with the activity of the Reunion hotspot. The central cone (2631 m a.s.l.) of the volcano lies in a caldera-like depression called the Enclos Fouqué and characterized by two craters, Bory and Dolomieu. Bory crater is inactive and the smallest one, whereas Dolomieu is the active crater and was also the site of a large caldera collapse in 2007 (Michon et al., 2007). Piton de la Fournaise is one of the most active volcanoes in the world (Bachèlery et al., 1982) with a mean time between consecutive eruptions during the past two centuries of 10 months (Stieltjes and Moutou, 1989) and at least 125 eruptions during the last century (30 eruptions since 2000). Most of the eruption occur along fissures inside tje Enclos Fouqué. The volcano has been monitored since 1979 from a permanent observatory that since 1999 has recorded continuous seismic and deformation data. Since 2009, new broad-band seismic and GPS stations have been deployed under the framework of the UnderVolc research project and the continuous seismic waveforms are publicly available by standard netdc request.

2.1 Geophysical and Geological information

In order to infer the possible scattering mechanism responsible for the local effect under investigation we must have some knowledge about the inner structure of Piton de la Fournaise volcano. Most of the information collected here has been taken from the Lénat et al. (2012) article, where they propose a general model of the volcano using information from geological and geophysical studies carried out in Piton de la Fournaise since the 1970s (a detailed list of references can be found there). They make a graphical compilation of all available geophysical information along a W-E profile and construct a geological section that integrates both the geophysical and geological information (see Fig. 5).

Starting at depth, the crust is relatively well defined by the reflection and refraction seismic data. The lithosphere is not significantly flexed and the crust is underlain by an under-plating body, which might represent the deep magma reservoir for La Rèunion volcanism. The early volcanic constructions above the oceanic crust pre-date Piton de la Fournaise. They can be attributed to the two large primary volcanoes, Piton de Neiges and Les Alizes volcano (see figure 3), but the location of the hypovolcanic intrusive complex of the latter implies that most of the the deep construction in this area should be composed of Les Alizes products.

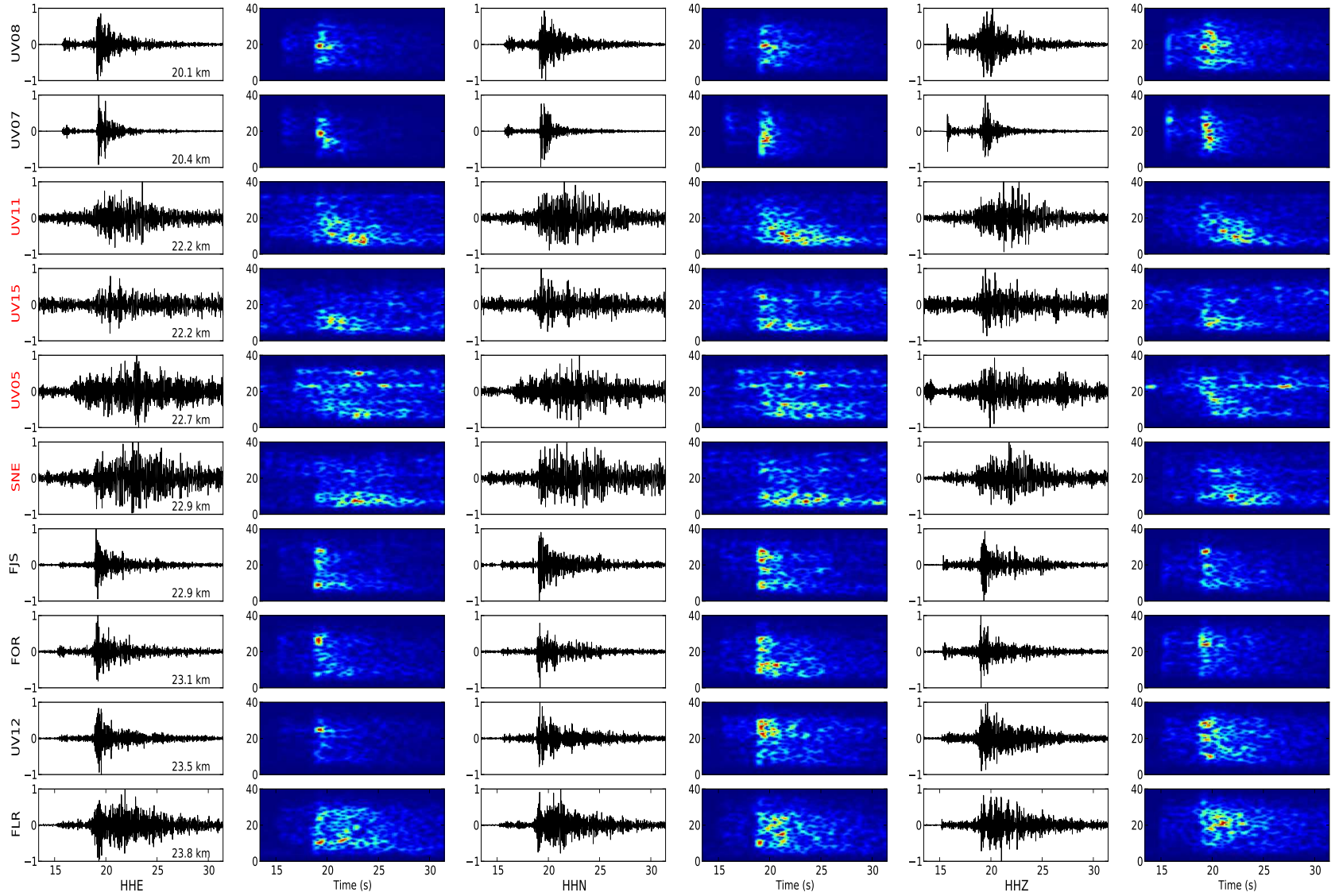

Fig. 2: Ten three component velocity seismograms (each trace has been normalized by its maximum amplitude) and spectrograms of the stations located nearby the summit. The stations are indicated on the left and the component in the bottom of the figure. The distance to the source is indicated on the right of the seismic E component trace. The stations located right on the summit (highlighted in red) exhibit a very distorted seismogram with no clear P- and S-wave onset and the energy shifted to later times. The spectrogram for these stations exhibit a reduction in the frequency and a more distributed over time frequency content.

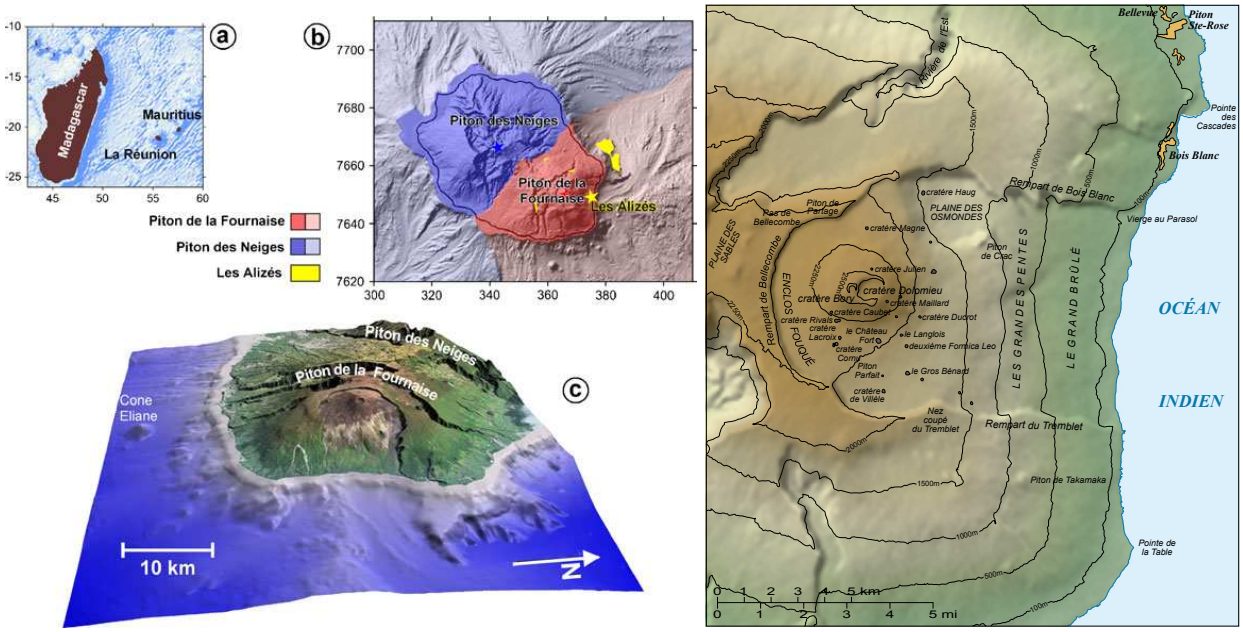

Fig. 3: Left: a) Location of Reunion Island in in the Indian Ocean, b) extent of the surface products of the three volcanoes of Reunion superimposed on a shaded relief map of the subaerial and submarine parts of the island (the stars show the centers of the volcanoes), c) oblique view of Piton de la Fournaise (Lénat et al., 2012). Right: Topographic map of Piton de la Fournaise indicating some important structures (wikipedia).

It is assumed that the base of the Les Alizes hypovolcanic complex lies at least at the top of the oceanic crust and that it has grown upward, along with the edification of the volcano. The earthquakes on the eastern flank are mostly located in the portion attributed to the Les Alizes construction but do not occur in the dense hypovolcanic complex (a brief discussion about Piton de la Fournaise seismicity is made in 2.2). The latter seems to act as a stress barrier.

According to the geological reconstruction, PdF started to grow around a focus located beneath the Plaine des Sables (west to the current volcano, see figure 3 right). The center has moved relatively recently to its current location, possibly passing via an intermediate position. The dense, high-velocity body beneath the Plaine des Sables and the western part of the Enclos probably corresponds to the hypovolcanic intrusive complex that developed before the volcanic center shifted to its present-day position. In Fig. 5 down it has been represented in blue the part of the complex inferred to have formed when the volcanic center was below Plaine des Sables, in orange the part that may have formed below the intermediate location, and in red the present magma conduit. Contrary to the Les Alizes complex, it is assumed that the base of the complex is not at the oceanic crust because PdF started to grow on a preexisting edifice. The March 1998 seismic pattern, with the root of the swarm at about the top of the crust, and the hypocentre column offset to the west of the summit, can be tentatively used to constrain the present and past deep structure. Magma reservoirs may have existed, and may still exist, at the mechanical and density interface between the oceanic crust and Les Alizes edifice. These reservoirs might have followed (or their migration may have caused) the eastward migration of the volcanic centers.

The zone of the presumed interface between Les Alizes and Piton de la Fournaise volcanoes must correspond to a specific lithology. It coincides with a marked velocity gradient, and during the March 1998 seismic swarm the pattern of the seismicity changed dramatically when the earthquakes reached this elevation. The hypocenters shifted to the east, in and above the zone beneath the summit, where a shallow reservoir is inferred to exist. The exact location, depth, volume, and shape of this reservoir are yet to be definitely established, as well as whether there are several separate reservoir units or a single one.

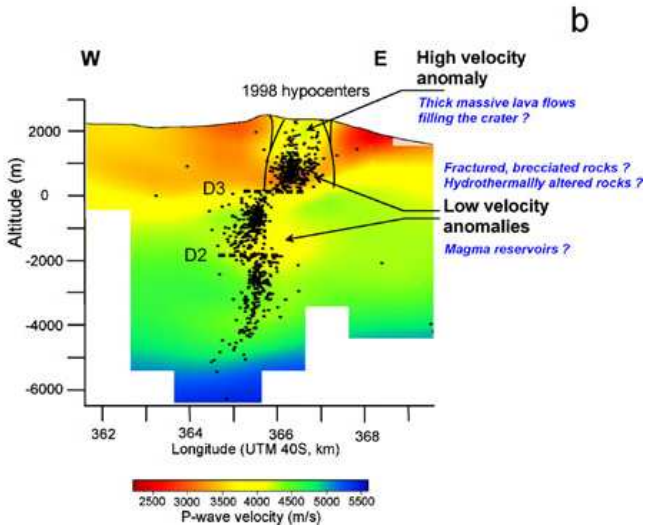

Fig. 4: W-E section in the P wave tomography from Prôno et al. (2009) showing March 1998 hypocenters. D2 and D3 are low seismicity regions located at the base of the two low-velocity zones (Battaglia, 2001).

The internal structure of the eastern flank of PdF is poorly known because access to this zone is difficult and it has therefore hardly been investigated by ground geophysical methods. The surface is entirely covered by recent lava flows.

The central active zone has been studied in more detail than the other zones (figure 4). The dominant structural feature of this zone is a collapse structure beneath the summit craters, above the inferred magma reservoir near sea level. It has been suggested that the collapse column constitutes a major mechanical heterogeneity and behaves as a trap for the seismic, intrusive, and hydrothermal activities because of its higher permeability and its weaker mechanical strength. In detail, the column is not homogeneous at a small scale. A positive seismic velocity anomaly extends from the near surface to about 1000 m asl. Below, down to about sea level there is a relatively low-velocity zone. A second low-velocity anomaly is located between about 1000 and 2000 m bsl. The two low-velocity zones are separated by a relatevely high-velocity volume, at about sea level with a strong velocity gradient suggesting the presence of a prominent mechanical vertical transition.

We point out that most of the shallow central structure of PdF remains still under discussion. As it has been suggested by Zecevic et al. (2013) the scarcity of LP seismicity on PdF could shed some light concerning its shallow structure. The lack of LP events might be explained by: (1) the non-existence or, if it exists, non well-developed hydrothermal system as that on Kilauea. (2) The lack of a shallow, low velocity layer. Note that whereas volcanoes such as Etna show a very shallow, low velocity layer, with P-wave velocity no more than 1800 m/s in the top 400 m due to the presence of poorly consolidated material (Saccorotti et al., 2004), the cone of PdF volcano is composed of layers of stiff basalt (Peltier et al., 2009)(with an average P-wave velocity greater than 3000 m/s (Battaglia et al., 2005)). Anyway, it has not been clarified yet if a shallow, low velocity layer exists on PdF. A detailed near-surface velocity model would be extremely useful to clear up some of the questions regarding this singular scarcity of LP events on PdF.

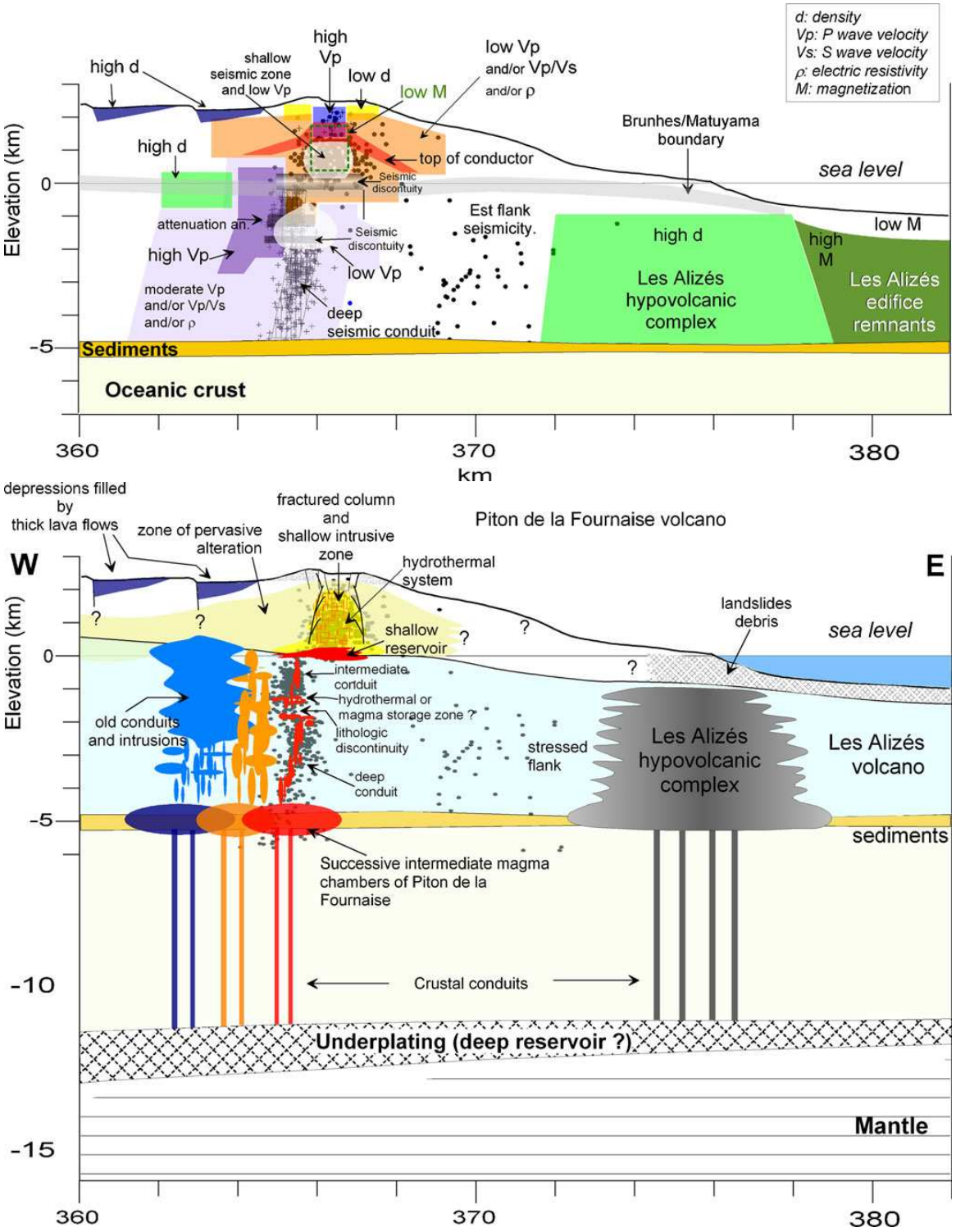

Fig. 5: Up: Graphical compilation of available geophysical information along a W-E profile. The geophysical structures have been represented with simplified and stacked within the figure. Down: Interpreted W-E geological section of Piton de la Fournaise based on geophysical and geological information. Horizontal coordinates: UTM km WGS84. (Lénat et al., 2012).

2.2 Seismicity

Lénat et al. (2012) provides an overview of the seismicity in Piton de la Fournaise since 1980. Three major zones can be identified. *One*, extending from about -6 km to sea level, is located slightly to the west of the summit. It is a column-like structure in which a clear upward migration of the quakes has been observed before the March 1998 eruption (Battaglia et al., 2005) and interpreted as the transfer of magma from a deep reservoir to a shallow reservoir inferred to exist near sea level, beneath the summit. A *second zone* exists beneath the eastern flank and since July 1985 has been subsequentely activated during certain crisis; it is generally regarded as being caused by the tendency of the edifice to move in the direction of its free flank. The *third zone* is located between sea level and the surface, beneath the summit craters. It is the most active zone and sistematically triggered during both inter-eruptive periods and pre-eruptive periods (Battaglia et al., 2005) with the largest proportion of events located in the upper low-velocity zone. It should be noted that, on the larger scale if the island, a deeper (10-30 km) and widespread weak seismicity is also recorded, but it is poorly located with the Piton de la Fournaise network.

In order to model the effect of high-resolution topography we must focus on high frequency recordings making use of the broadband seismic network deployed since late October 2009 as part of the Understanding Volcanoes (UnderVolc) project. It would be desireable to have available a large number of events distributed all within the volcano down to a few kilometers depth. Fig. 6 shows a representative picture of the shallow seismicity in PdF along one year (2011). As it has already been pointed out the swarms are predominantly concentrated about sea level elevation under the summit, corresponding to the high-seismicity zone. Conforming depth increases events are becoming more rare. Looking at the flanks of the volcano we find a very few events located under Le Grandes Pentes in the eastern flank.

Note that according to Battaglia et al. (2005) (1) the attenuation mainly affect to earthquakes located deeper than 1 km bsl. The reduced number of events whose hypocentral depth ranges from 0 to a couple of kilometers bsl make us look for deeper quakes. Thought these very deep events might not be model in our simulations (it would imply computationally very expensive simulations due to the large numerical domain involved), they will considerably enlarge the ray coverage and hence shed more light on the scattering phenomenon. —-> Introduce a figure with the events used in this study??????. —> Mention a lot of events available for shallow depths.

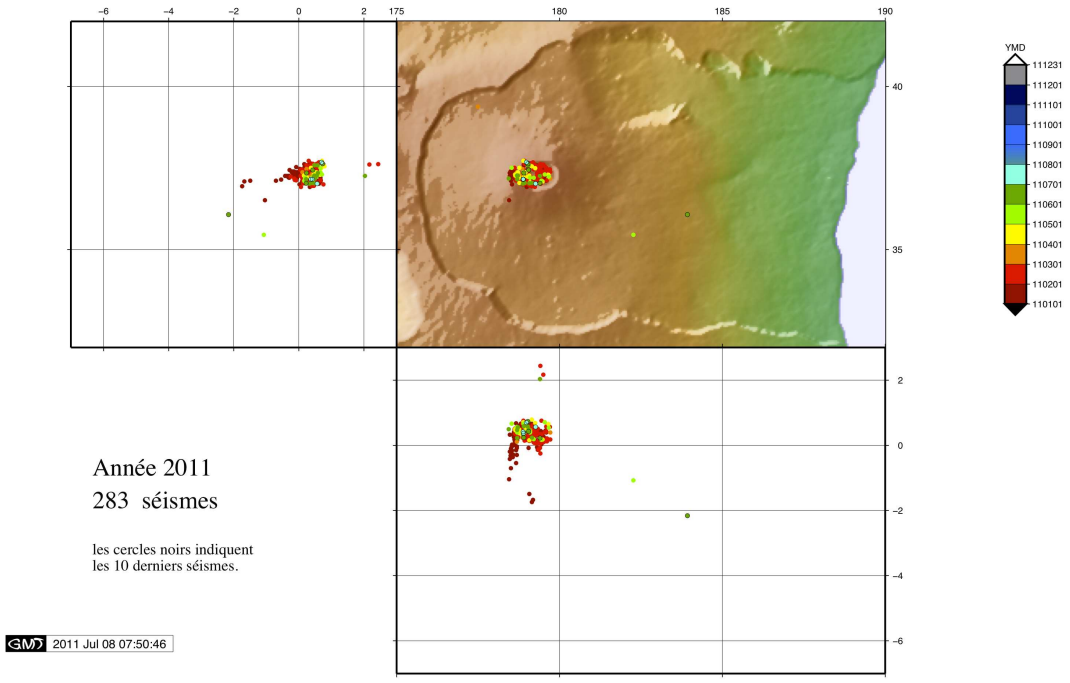

Fig. 6: Piton de la Fournaise shallow seismicity during broadband seismic instrumentation (2010, 2011 and 2012). From Observatoire Volcanologique du Piton de La Fournaise.

3 Data processing

Detailed next is the data processing we have applied as well as a brief description of the seismic observables chosen to feature the phenomemon. Broadband data has been provided by the Observatoire Volcanologique du Piton de la Fournaise (Institut de Physique du Globe de Paris) via standard netdc request. Most of the events selected with a high signal-to-noise ratio occurred in 2010 (just a few of them belong to 2011) during the YA temporal network deployment consisted of 21 seismic stations. Since we want to focus on a limited area nearby the summit of the volcano, we just select a set of 11 stations located close around to the Dolomieu crater. ——> Show the stations selected for this study???????.

After the instrumental correction, a pass-band filter between 5 and 30 Hz has been applied to the seismograms, previously ensuring throught the spectrogram that the signal is basically concentrated in this range (the lowest frequency filter has been chosen because of the high level of low-frequency noise presents up to 5 Hz). In all the figures shown below the seismograms have been sorted by the source-receiver distance and each trace normalized by its maximum amplitude in order to make visually more comparable the waveforms.

We describe now seismic observables we have used to feature the phenomenon:

1. Maximum amplitude (max_amp): We compute the maximum amplitude scaled with the hypocentral distance to account for geometrical spreading. This observable is manifested as a crucial one because the maximum amplitude of the seismogram drops off when strong attenuation, either apparent or intrinsic, is present. We point out that the energy has been also tested, showing a similar behaviour than the maximum amplitude.

2. Mean value of the envelope (mean_env): The mean value of the envelope changes significantly when the seismogram is quite distorted, showing large values continuously all along the seismogram. In the case of a no distorted seismogram with clear P- and S- wave arrivals, large values of the elongation are

just concentrated around the onsets whereas the rest of the seismogram shows low amplitudes. Point out that this parameter must be computed after the normalization of each trace by its maximum value has been done.

3. Center frequency (cfreq): We obtain the center frequency by computing the first moment of the power spectral density function:

$$f_c = \frac{\int f P(f) df}{\int P(f) df}$$

It is a measure of the frequency where the power is concentrated. The dominant frequency has been also tested, computed as the second moment of the power spectral density, revealing a similar behavior than the center frequency. However the latter one provides lower values when the bandwidth is wide and the frequencies are not quite concentrated in a narrow frequency range. We compute the center frequency for each component and from them the mean value.

The seismic observables described previously have been computed once we have windowed the seismogram. The P-wave onset and the end of the trace have been picked manually rather than using a STALTA trigger because the signal-to-noise ratio for the stations located on the summit is not often so favorable and the trigger does not pick the P arrival accurately.

Some other seismic observables have been considered such as bandwidth, signal length???????.

4 Results: Extracting features

In order to study how the parameters mentioned above vary with depth we separate the set of events into three major depths; shallow events ranging from 1320 m asl down to 160 m bsl, intermadiate events (540-2100 m bsl) and very deep events (8770-25170 m bsl). The value of the seismic observable for each event has been normalised by the mean one considering all the stations.

(((We will first visualize intermediate deep events in order to illustrate clearly the effect. Then we will move up to shallow events where the fact of working with shorter distances make more difficult a distinction between different stations. Finally we will go back to deep events in order to study several angles of incidence of the ray with respect to the summit.

All the figures have been attached here `http://www.geophysik.uni-muenchen.de/~amolina/`, we plot just Z component (it has been tested a similar behavior for the other two components) and they are sorted by distance. The seismogram for each station is plotted on the left and spectrogram on the right (the name of the station is located vertically in the middle). The parameters we work with are plotted as well, alike the receiver-source distance (beneath the seismogram). The value out of the brackets represent the absolute one for each station, that one in brackets represents the factor with respect to mean one (obtained from meaning all the stations on and around the summit). Considering the three parameters it means: values smaller than 1 for the maximum amplitude represent a reduction of the amplitude of this station with respect to the mean one, values larger than 1 in the mean envelope represent seismogram more distorted than the mean one and values smaller than 1 in the center frequency represent a reduction of this paramenter for this station with respect to the mean one.

Shallow events

Shallow events (1320, 1160, 980, 770, -160):

Starting from quite shallow events we reach a maximum depth of about 200 m bsl. These events correspond to the high-seismicity zone and most of them are located in the northern side of the crater (see Fig. 7).

All these shallow earthquakes can be classified as volcanic-tectonic type B events (an example has been shown in Fig. 7). Most of the stations do not show distinction between P- and S-wave onset, it is generally impossible to detect any clear S-wave arrival. As the heterogeneity in a volcano concentrates essentially very shallow there will be a large amount of scattering in the wave propagation path independently of the source-receiver geometry. We must also take into account that due to the short source-receiver distance compared

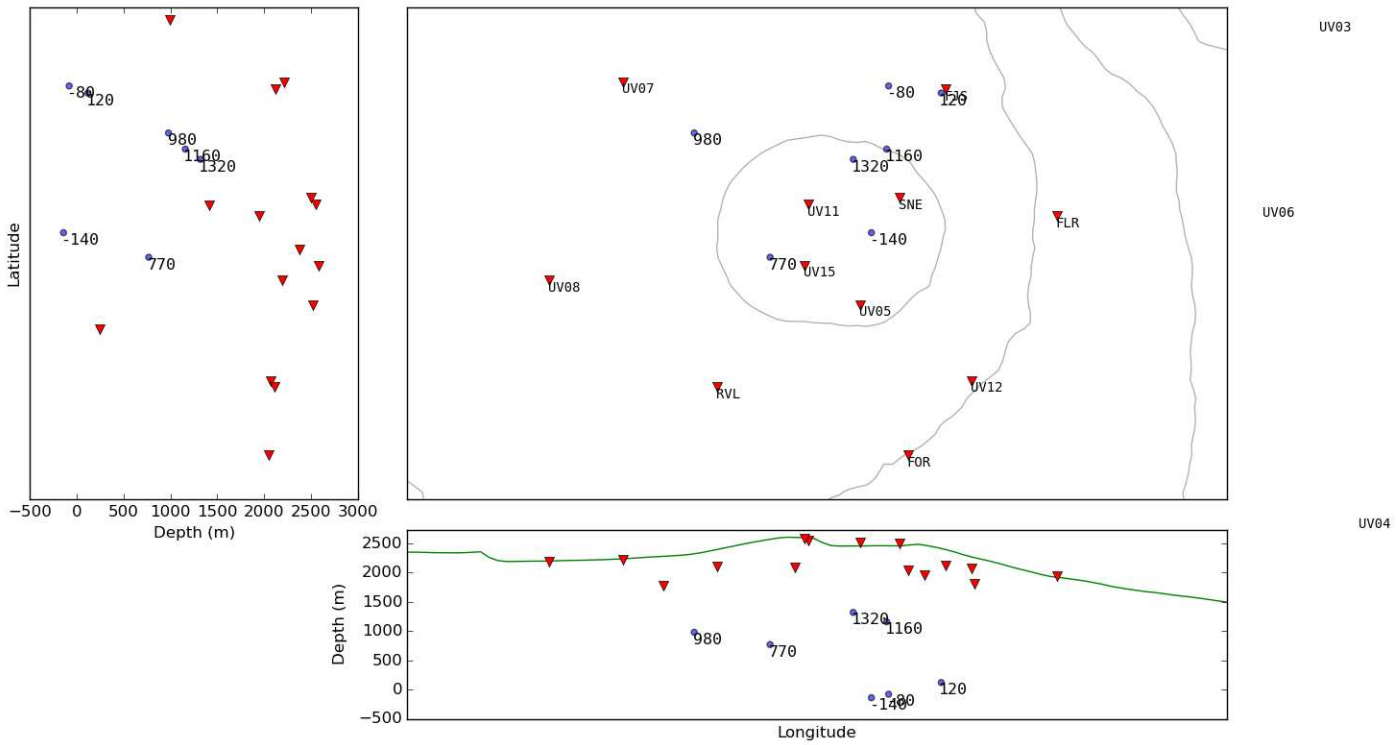

Fig. 7: Shallow events in blue circles, stations in red triangles.

to the dominant wavelength (200 m for a dominant frequency 20 Hz and a velocity wave propagation of 4 km/s), the near-field seismic wavefield cannot be ignored. The seismograms in figure 7 show quite a similar aspect for all the stations. The waveform seems to exhibit a more distorted waveform as distance increases.

In figure 8 we compare the seismic observables for all these shallow events (the values have been normalised by the mean value obtained from all the stations). For the case of the maximum amplitude we distinguish that while for some stations these values range in a wide interval, for others they show low and quite concentrated values. Among these latter stations are included those ones located closest to the summit. When we consider the center frequency only the stations closest to the summit seem to be affected by a reduction (middle image in 8). The mean value of the envelope does not respect this tendency.

Intermediate events

The depth for these events ranges from 540 m to 2100 m bsl, distinguishing two regions; the region below the summit and that one below Les Grand Pentes in the eastern flank of the volcano (see figure 11).

Below the summit (-540, -750, -1040, -1190, -1670)

For the events deeper than 500 m bsl we start distinguishing visually the path effect (in figure 17 we plot -1670 event). We differentiate the waveforms more distorted (stations SNE, UV11, UV15 and UV05). Looking at the parameters we observe that the stations on the summit exhibit a considerable reduction of the amplitude, seismograms much more distorted revealing high values for the mean envelope, but mainly it is the center frequency the observable that most changes. We point out that some other stations show low values of the maximum amplitude but just the stations on the summit exhibit a reduction of the center frequency and an increase in the mean envelope.

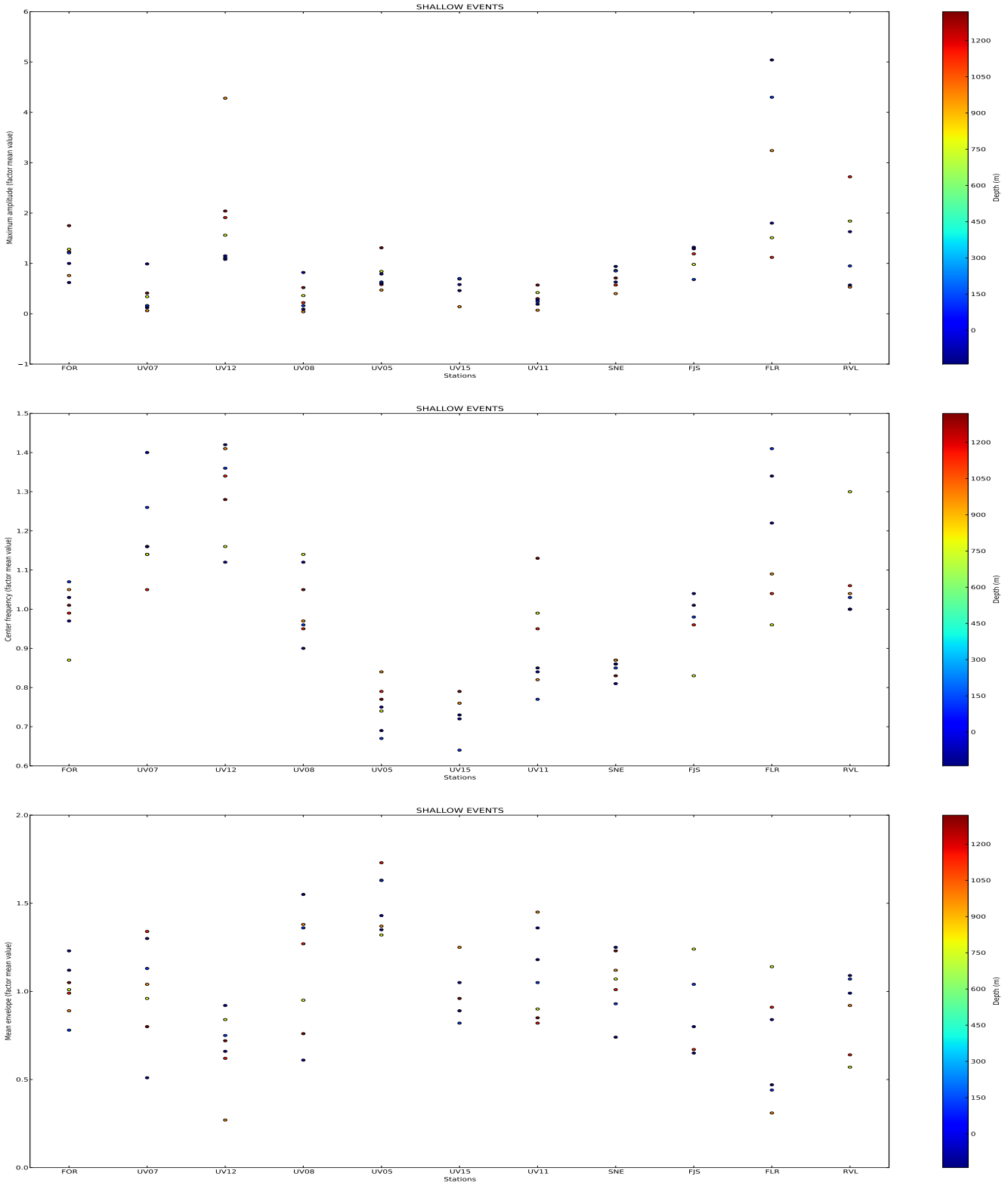

Fig. 8: Maximum amplitude (up), center frequency (middle) and mean envelope (down) for the shallow events (parameters normalised by the mean value). Maximum amplitude show low and more concentrated values for the stations close to the summit thought there are some other stations affected as well, center frequency show low values just for the stations on the summit. The mean value of the envelope does seem to follow this tendency.

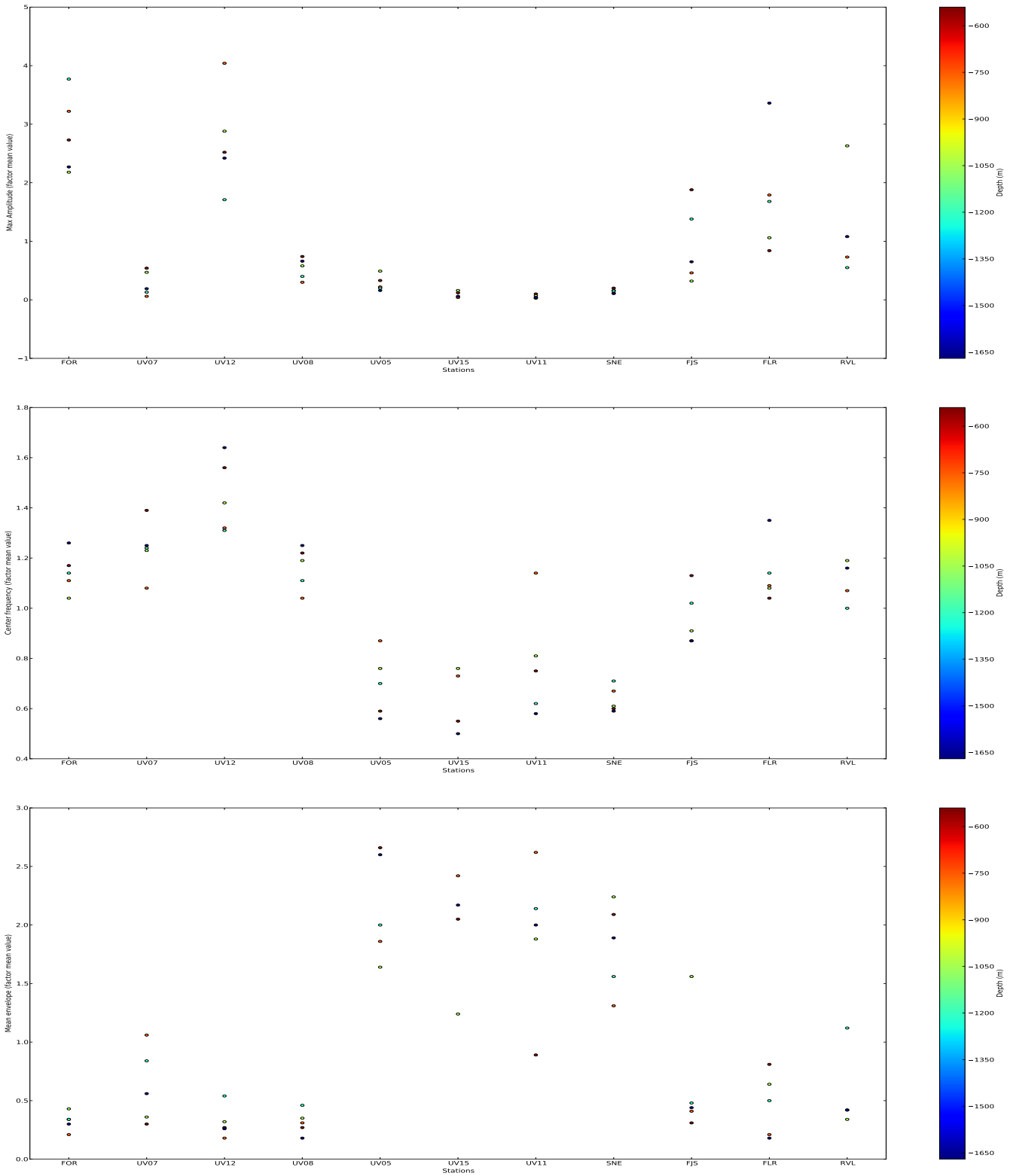

Fig. 9: Maximum amplitude (up), center frequency (middle) and mean envelope (down) for the intermidiate events located beneath the summit (parameters normalised by the mean value). Maximum amplitude show low and more concentrated values for the stations close to the summit thought there are some other stations affected as well (UV07 and UV08), center frequency and mean envelope show low values just for the stations on the summit.

Below Les Grand Pentes (-1830, -2080, -2100)

For these three events located below Les Grand Pentes the effect emerges again for the stations on the summit concerning the maximum amplitude and the mean envelope (notice that it even happens when the incidence is quite lateral). However now the values are not so distant from the average ones (see figure 10) and there is some important variation among the stations on the summit (those ones located on the western flank seem to be more affected). The center frequency does not exhibit the normal reduction for the stations on the summit. We point out that there are not available much data in this zone and the data available shows a defficient signal-to-noise ratio, it makes difficult to consider just these three events as representative.

Very deep events

See figure 14.

Western flank (-8770, -11040, -14270, -15560, -15600, -18840, -20100)

For these events we recover values quite distant from the average ones. Again note that even for a very lateral incidence the effect remains quite significant. It may suggest that the scattering zone is located quite closed to the surface below the summit.

It has been tried to distinguish some influence of the hypothetical scattering zone on some stations which though are not on the summit the seismic ray coming from the source may pass through, but there is not a clear influence observed. As it has been pointed out it could probe as well the very shallow location of the scattering region.

The station more affected with this incidence is UV05 (this fact agrees with the incident trajectory) which signal is sometimes so low that the presence of the noise perturbs some seismic observables.

Eastern flank (-10910, -14240, -17190, -25170)

When we have an incidence from the east of the summit again stations located on the western flank (UV07 and UV08) are affected concerning the maximum amplitude. It might be due to either the magma deep conduits placed below the western flank or some depressions filled by thick lava flows (see figure 5). Concerning the center frequency stations on the summit exhibit quite varied values. This might result from the low signal-to-noise ratio for these events, as it can be distinguished in the mean envelope values since the stations on the summit reach very high values.

Ray trajectories

In order to delimit the region that it is supposed to act as a scattering body we propose to include in a 3D model of the volcano the receiver-source ray trajectories for those cases in which it is clear the already mentioned effect. The table 1 depicts the stations for which the three study parameters show a more separated value from the mean ones. In the table we specify this factor between brackets for each station, not indicating the integer digit. In blue color we find the stations located on the summit, in red the stations which finally have been selected for each event to trace the ray source-receiver trajectory. The criterion to select them is the fact that they appear simultaneously in the three columns so they show a very clear effect, affected in the three ways: reduction of the amplitude, distortion of the seismograms and lack of high frequencies. The threshold values to include the stations at each column have been specified in the first row of the table 1.

The table 1 illustrates how conforming the depth increases the stations on the summit start occupying more generally the three columns, working with deeper events (VT type A) the differences between the stations on the summit and the rest get accentuated.

Figure 15 show two images with different perspectives of the ray trajectories in a volcano topography model (16 x 16 km with 250 m resolution). In order to have some reference bodies we include the hypothetical shallow reservoir located at sea level (a circle plane with 2000 m of radio) and the conduits located below the western flank (2000 m of radio and 5 km height). It shows the source-receiver traces for those cases in which

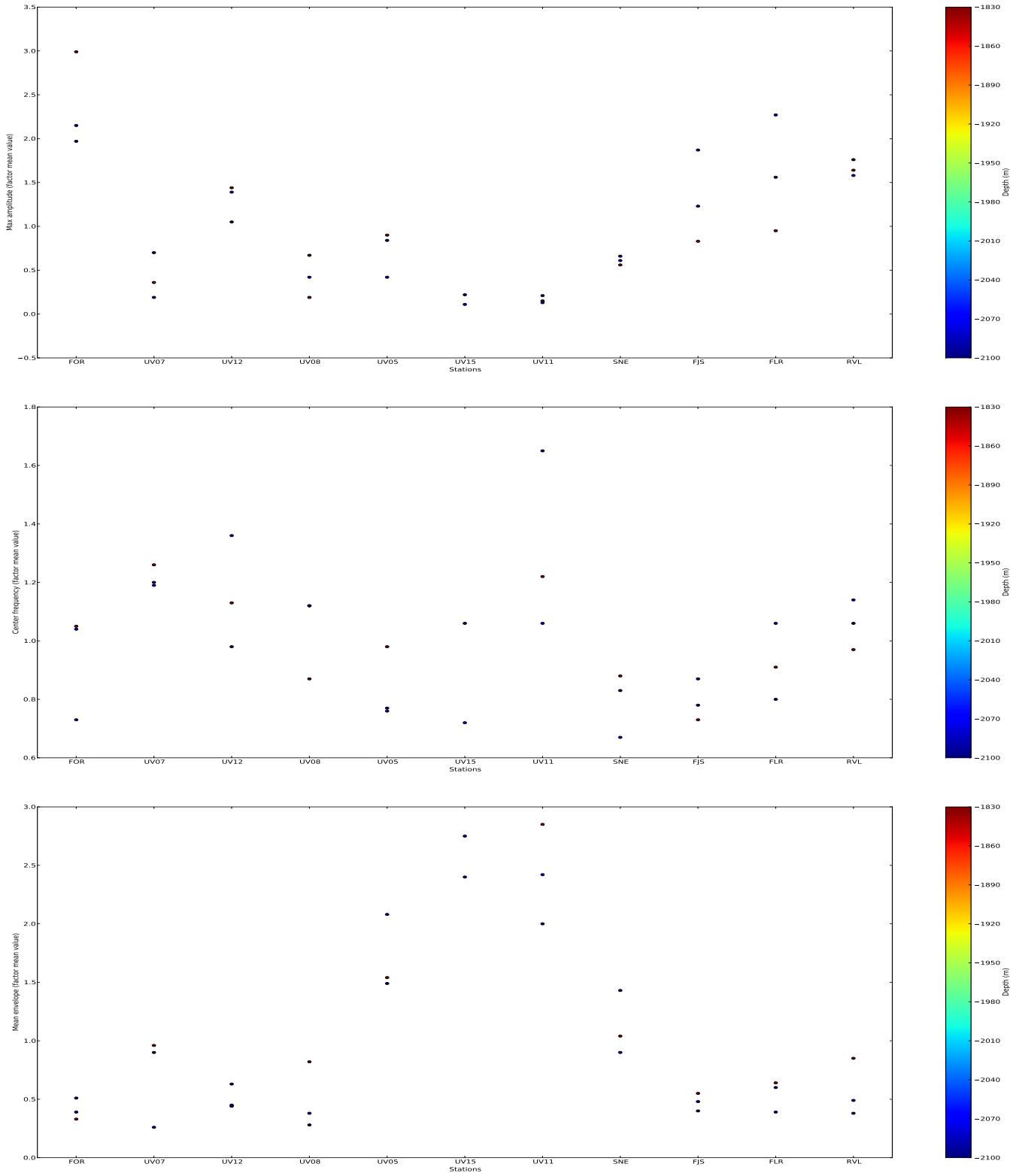

Fig. 10: Maximum amplitude (up), center frequency (middle) and mean envelope (down) for the events located beneath Les Grand Pentes (parameters normalised by the mean value). Maximum amplitude and mean envelope respect the tendency already mention with the exception that now the station on the western flank seem to be much more affected. Center frequeny does not follow the tendency.

Depth(m)	Amp(0.8)	Mean_env(1.1)	Center freq(0.9Hz)	Sel. stations
		SHALLOW EVENTS	(UNDER THE SUMMIT)	
1320	UV09(.3)UV07(.4)UV11(.6)UV15(.7)	UV15(.13)	UV05(.87)SNE(.88)FOR(.90)UV15(.92)	UV15
1160	UV07&UV09(.1)UV11(.3)UV05&SNE(.6)	UV09(.35)UV11(.17)UV05(.07)	UV05(0.87)SNE(.91)UV11(.93)	UV05 UV11
980	UV11&07&08(.1)UV09(.2)UV15(.3)	UV05(.19) UV09(.15)UV11(.14)	UV11&UV08(.89)UV05(.94)UV15(.95)	UV05
770	UV08(.5)UV11(.6)SNE(.8)	FOR(.29)UV12(.10)	FOR(.82)UV05(.83)FLR(.92)SNE(.95)	-
120	UV07(.2)UV11(.3)UV05(.6)UV15(.7)	UV05(.14)FJS(.12)UV11(.08)UV15(.07)	UV05(.81)UV15(.85)UV11(.87)	UV05 UV11 UV15
-80	UV11(.2)SNE(.5)UV15(.6)UV05(.7)	UV11(.43)RVL(.29)UV05(.23)UV15(.19)SNE(.16)	UV05(.83)UV15(.85)UV11(.86)RVL(.88)SNE(.92)	UV05 UV11 UV15 SNE
-140	UV07&08(.1)UV11(.2)UV09(.3)UV15(.5)UV05(.6)	UV05(.33) UV11(.28)UV08(.14)	UV05(.84)UV08(.85)UV11(.89)UV15(.92)	UV05 UV11
		DEEP EVENTS	BELOW THE SUMMIT	
-540	UV11(.1)SNE&UV15(.2)UV05(.4)UV07(.6)	UV05(.28) UV12(.16)UV09(.15)UV11(.05)SNE(.04)	SNE(.62)UV05(.69)UV15(.78)UV11(.89)	UV05 SNE UV11
-750	UV11(.0)SNE&UV15(.1)UV05(.3)UV09(.4)	UV05&UV11(.16)SNE(.14)	SNE(.85)UV07(.88)UV15&UV11(.89)	SNE UV11
-1040	UV11(.1)SNE&UV15(.2)UV07(.5)UV09&UV15(.6)	UV05(.24)UV12(.10)UV15(.09)SNE(.06)	SNE(.65)UV05(.85)UV11(.86)UV15(.87)	SNE UV11 UV05 UV15
-1190	UV11(.0)SNE&UV07(.1)UV05(.2)RVL(.5)	RVL(.46)UV05(.44)UV11(.26)	UV11(.73)UV05(.76)SNE(.84)	UV11 UV05
-1670	UV11&UV15(.0)SNE(.1)UV05(.2)UV07(.3)	UV05(.43)SNE(.19)UV11(.13)	SNE(.69)UV05(.72)UV11&UV15(.77)	UV11 UV05 SNE UV15
		DEEP EVENTS	BELOW LE GRAND PENTES	
-1830	UV11(.1)SNE&UV09(.5)	UV11(.33)FLR(.11)UV12(.11)	UV11(.83)FJS(.90)SNE(.92)	UV11 UV05
-2080	UV11&UV15(.1)UV05(.4)UV08(.5)SNE&UV07(.6)	UV12(.52)RVL(.32)SNE(.18)FJS(.13)UV11(.12)UV15(.09)	SNE(.80)FJS(.89)UV15(.90)UV05(.94)UV11(.96)	UV15 SNE UV11
-2100	UV07(.2)UV09(.4)SNE(.6)	SNE(.22)UV05(.20)UV12(.10)	FOR(.76)FLR(.83)FJS(.86)UV12(.91)	-
		VERY DEEP EVENTS	BELOW WESTERN FLANK	
-8770	UV11&UV15(.1)SNE(.3)UV05&UV08(.5)	UV05(.43)UV11&UV15(.41)SNE(.30)	SNE&UV05(.77)UV15(.82)UV11(.83)	UV05 UV15 UV11 SNE
-11040	UV11(.1)SNE(.3)UV08(.5)	SNE(2.76)UV11(1.68)	UV11(0.7)SNE(0.8)	UV11 SNE UV05 UV15
-14270	UV11(.1)UV15(.2)UV05(.3)SNE(.3)	UV05(.46)UV11(.40)UV15(.39)SNE(.33)	UV05(.71)UV15(.75)UV11(.79)SNE(.82)	UV05 UV15 UV11 SNE
-15560	UV11(.1)SNE(.2)UV05(.3)	UV05(.58)UV11(.22)RVL(.18)SNE(.17)	SNE(.78)UV11(.83)UV05(.84)	SNE UV11 UV05
		VERY DEEP EVENTS	BELOW NORTHWESTERN	
-15600	UV11(.1)UV05(.3)SNE(.4)	UV11(.78)UV05(.36)UV12(.14)SNE(.13)	UV05(.70)UV11(.78)SNE(.80)	UV11 UV05 SNE
-18840	UV11(.1)UV15(.2)SNE(.3)UV05(.4)	UV05(.68)SNE(.12)UV11(.10)UV15(.09)	UV05(.78)UV11(.80)UV15(.82)SNE(.83)	UV05 UV11 UV15 SNE
-20100	UV11(.1)SNE(.3)	UV11(.66)UV09(.37)RVL(.29)SNE(.15)	UV11(.76)SNE(.84)	UV11 SNE
		VERY DEEP EVENTS	BELOW EASTERN FLANK	
-10910	UV11(.1)UV15(.1)SNE(.4)FJS(.7)	UV11(.46)UV15(.33)FJS(.14)	UV15(.79)SNE(.83)UV11(0.85)FJS(.91)	UV11 UV15 FJS UV05
-14240	UV11(.0)UV05(.2)SNE(.4)RVL(.5)	UV11(.41)RVL(.17)SNE(.10)	UV11(.76)UV05(.77)SNE(.83)FJS(.94)	UV11 SNE
-17190	UV11(.1)UV15(.1)SNE(.5)	UV11(.67)UV15(.34)	UV15(.82)UV11(.85)SNE(.87)UV05(.90)	UV11 UV15 SNE
-25170	UV11(.1)UV15&UV05(.1)SNE(.5)	UV01(.63)SNE(.45)	FLR(.90)FOR(.93)	-

Table 1: Stations that exhibit more distant values from the mean one. The parameters have been described in section 3. Stations in blue are located on the summit. The last column include just those stations that are present in the three columns.

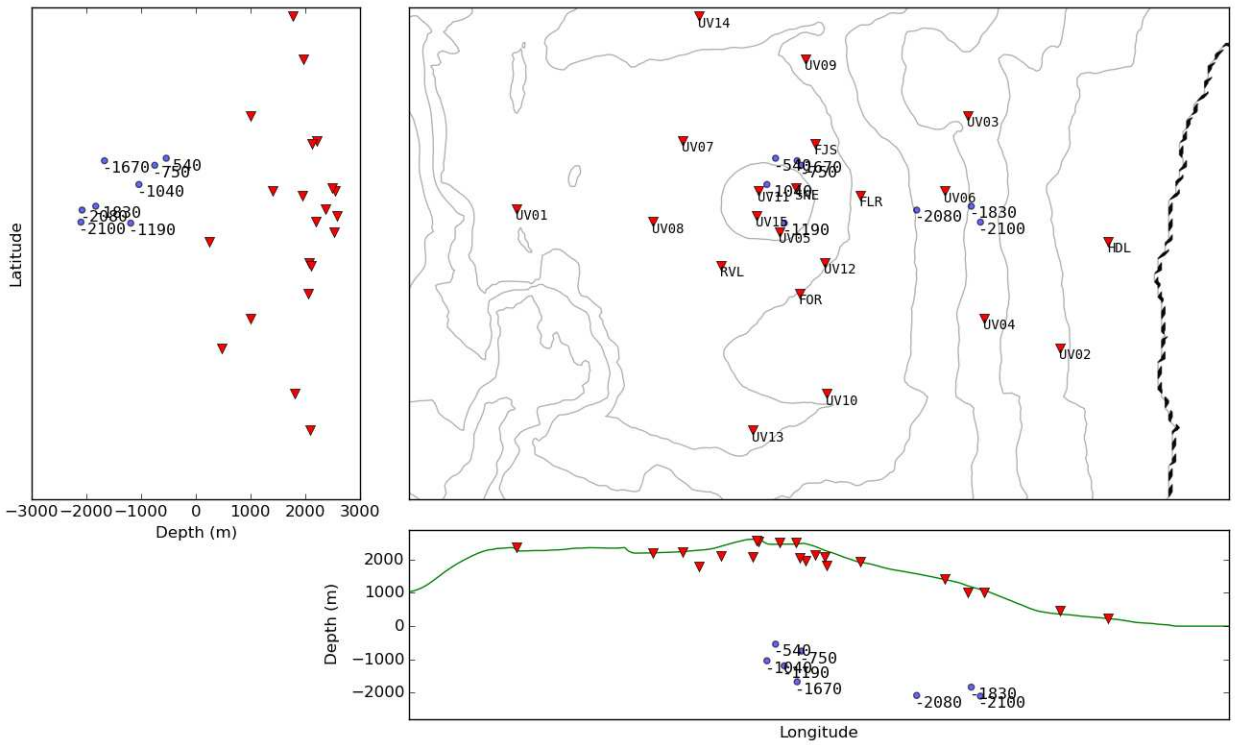

Fig. 11: Deep events in blue circles, stations in red triangles.

the effect studied is more clear (extracted from the last column in table 1). As it can be observed even with a very lateral incidence the effect remains for the stations located on the summit.

5 Discussion

If we pay attention to the source-receiver ray trajectories affected by the effect studied, we conclude that whatever is producing this dramatic change on the seismograms of the summit stations, it may be located quite shallow. It seems to be some influence of the inner structures of the volcano on some stations no directly located on the summit, but it is still difficult to infer that it can be associated to some structure already known. It arises three possible scattering mechanisms that may produce this effect:

1. Topography: The crater structure at the summit of Piton de la Fournaise exhibits strong topography variations. We must take into account that the 4 stations affected are located quite close to the border of the crater, so topography may play an important role. As it has been suggested in 2.1 the collapse column may constitute a major mechanical heterogeneity and behave as a trap for the seismic waves. Some previous studies concerning the effect of real volcano topography on seismic waves ((O'Brien et al., 2010)) confirm that the introduction of complex topography significantly distorts the seismic wavefield constituting the most important scattering mechanism. The presence of a steep and rugged free surface can also change notably the energy content of the seismograms ((Ripperger et al., n.d.)). However there are still a few questions arising from our results that should present some contradiction with this supposition:

(a) One general statement concerning the effect of topography is that mountain tops and ridges produce the amplifications of Peak Ground Velocity (PGV), awhile flat areas or plateus exhibit low values for the PGV. In our case we are observing the opposite effect. Furthermore, the time-frequency representation of the seismograms close to the summit should show a general trend of increasing mean frequency with increasing

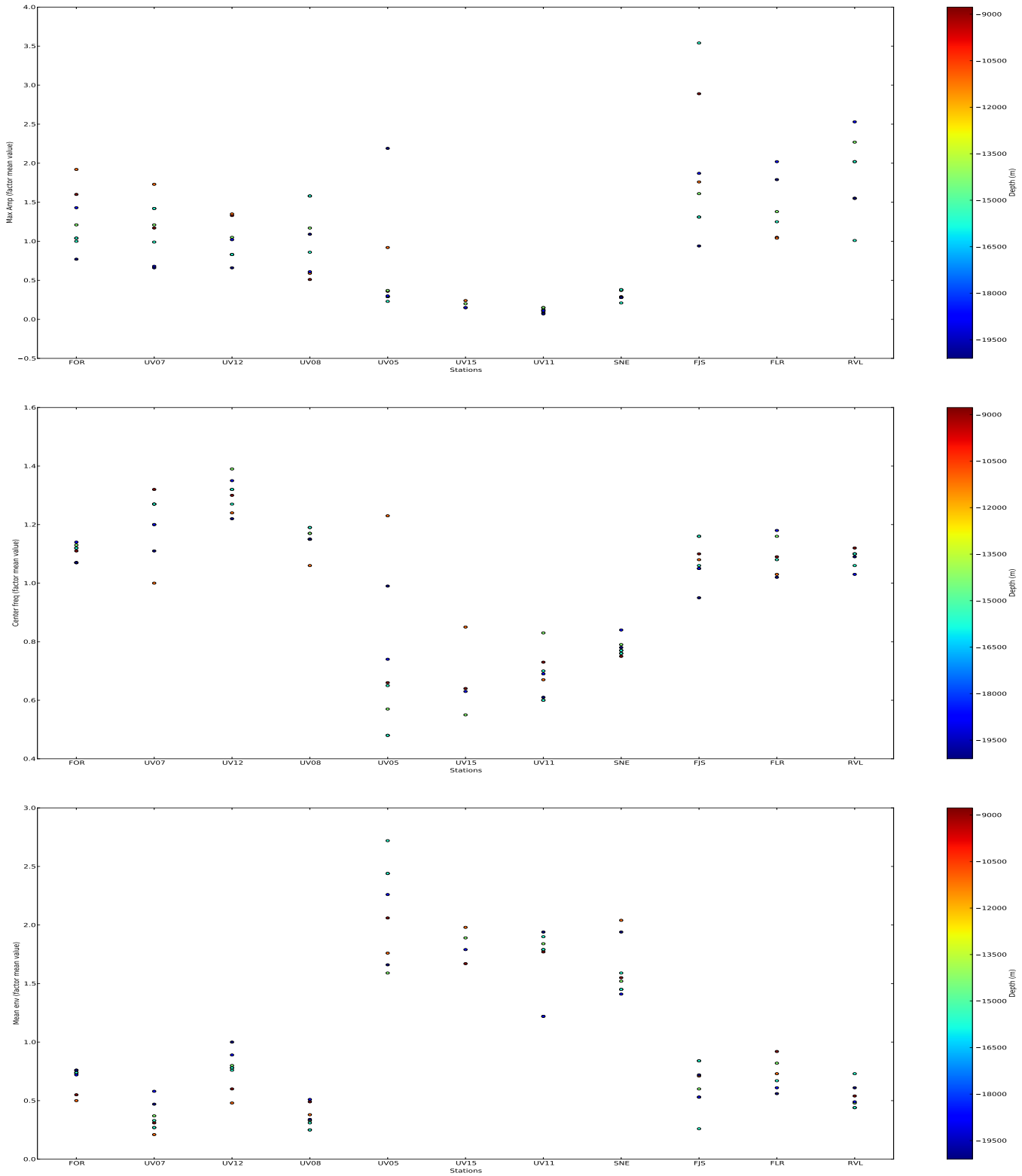

Fig. 12: Maximum amplitude (up), center frequency (middle) and mean envelope (down) for the events located beneath the western flank (parameters normalised by the mean value). High maximum amplitude, high mean envelope and low center frequency values for the stations located on the summit.

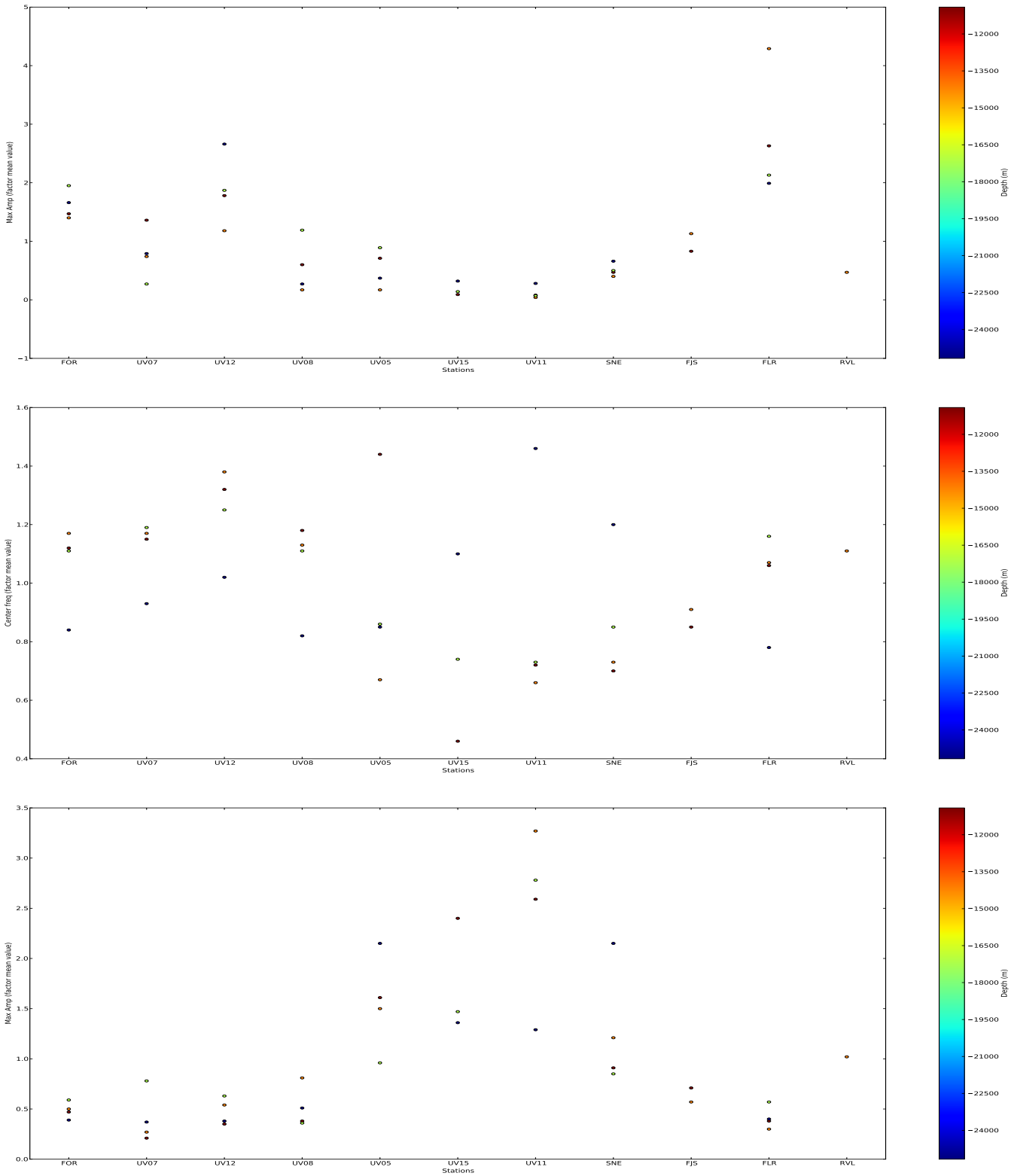

Fig. 13: Maximum amplitude (up), center frequency (middle) and mean envelope (down) for the events located beneath the western flank (parameters normalised by the mean value). Apart of the stations located on the summit some others are affected by an increase in the maximum amplitude value. Low signal-to-noise ratio for the stations located on the summit perturbs the values obtained for the center frequency and generate very high mean envelope values.

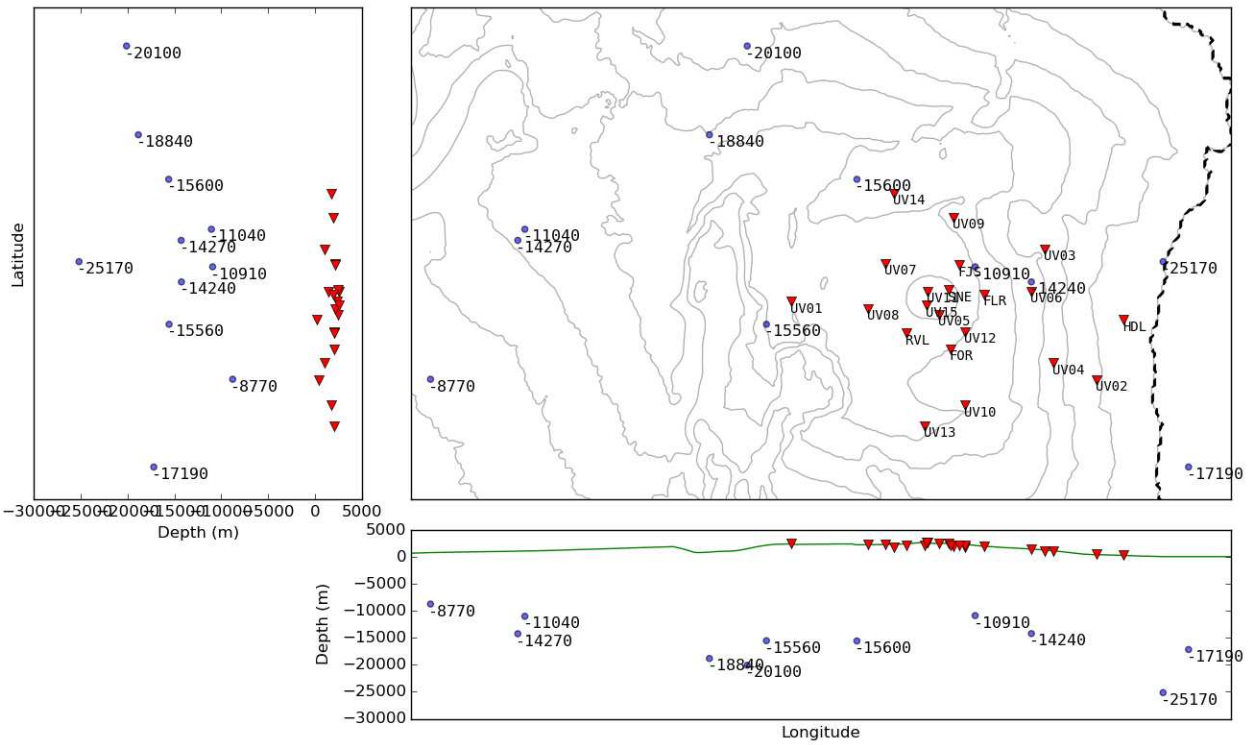

Fig. 14: Very deep events in blue circles, stations in red triangles.

time. The longer wavelengths are less sensitive to the topography and therefore are less prone to being trapped by these structures while the smaller wavelengths remain trapped for longer times. This should lead to a dominance of higher frequencies at later times, however for the stations on the summit the spectrograms exhibit clearly lower mean frequencies for longer times, an characteristic effect of intrinsic attenuation.

(b) Though there are some differences, all the four stations located on the summit exhibit a very similar behavior independently on the ray incidence, something that suggests that this topography works as a complete structure where more local variations are neglected.

2. Scattering produced by a very shallow scattering body: As seismic waves pass through a heterogeneous region, the waves are scattered, changing their velocity and attenuating them. This apparent attenuation is not true attenuation in that the seismic energy is only delayed to later in the seismogram and not changed to a different form of energy. This is in contrast to intrinsic attenuation where seismic energy is converted, by friction, into heat energy. The amount of apparent attenuation is dependent on the frequency of the seismic wave. The maximum amount of apparent attenuation occurs at frequencies where the corresponding wavelengths are on the order of the heterogeneity dimension.

Considering that what our seismograms mainly exhibit is a dramatic change in the frequency content (lack of high frequencies) and a shift to later times of the main part of the signal, apparent attenuation produced by some scatter located below the summit is a plausible explanation. Presumably this scatter body may contain magmatic fluids with high intrinsic attenuation as well. The cons against this possibility however is that very lateral incidences remain exhibiting this phenomenon and events located directly below the summit deep enough do not show more dramatically this effect than other coming very laterally. As it has been already exposed in the Geophysical Information section, other studies suggest a shadow seismic zone with low P-wave velocity, the extension of this zone should emulate a cylindrical hydrothermal system in the first 2 kilometers below the summit and a shallow flat reservoir located at sea level, but this structure does not

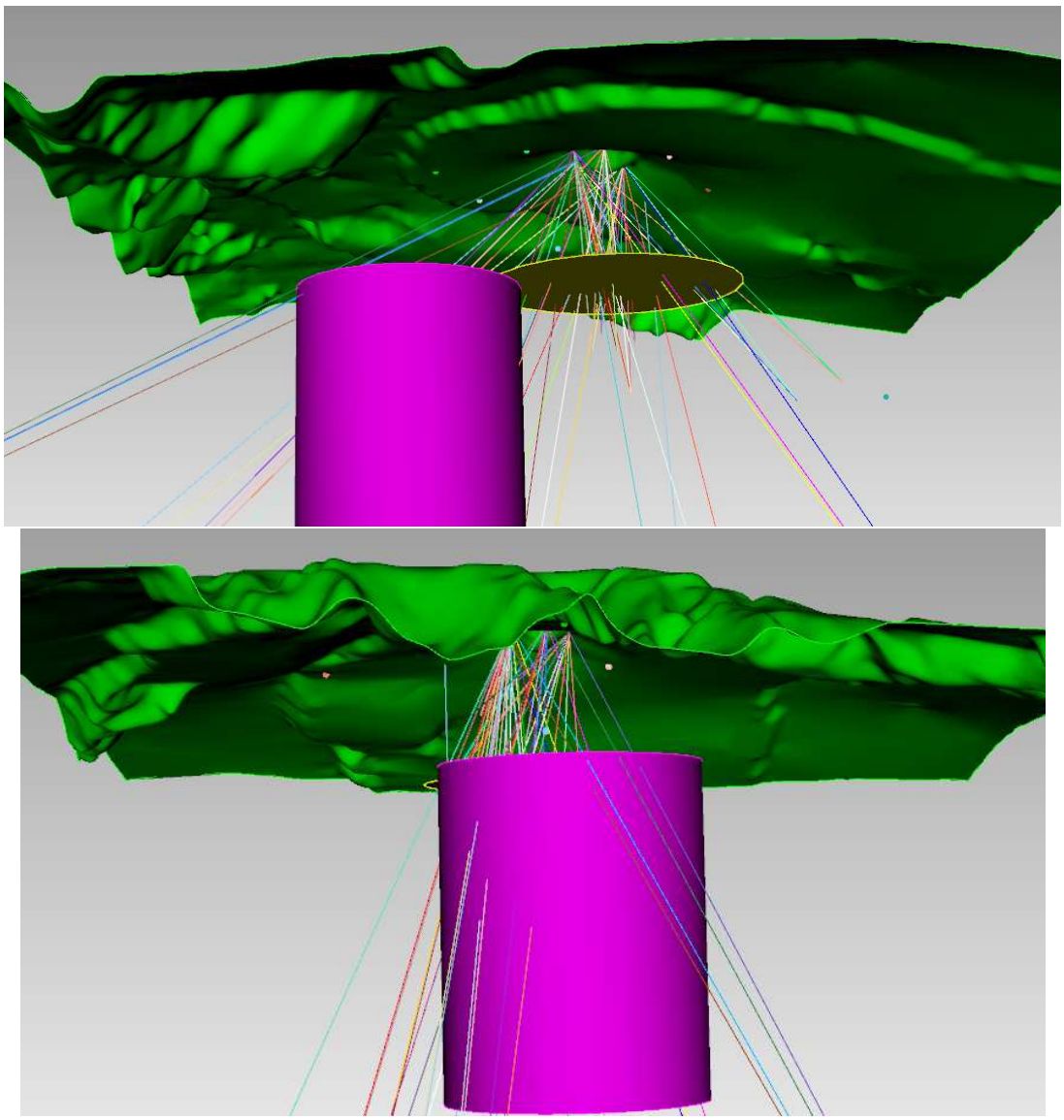

Fig. 15: (Up) E-W and (down) N-S view of the ray trajectories that have been selected for showing a very clear scattering effect.

seem to be inferred from the various ray trajectories considered in our study. Though apart of the stations located on the summit it has been observed a similar (but reduced) effect on some other stations, no clear dependency of this hypothetical structure can be inferred.

In addition to this, some other hydrothermal systems and intrusive conducts suggested by literature (like that one located below the Western flank) may work as possible scatters for the seismic traces coming very laterally.

3. Layering at the summit: Finally a very local layering structure with a high impedance may produce this effect. It would be consistent with very lateral incidences. However there is again some other cons against this option. Assuming a thin layer interface near the summit may produce the wave-train persists for much longer and the higher frequencies being trapped inside the structure for longer.

As it has been explained, no a single scattering mechanism may justify completely the behavior observed and there is no doubt that at some point all of them mentioned participate as scattering actors. On the other hand, there is still some work missing concerning the characterization of the effect, it is necessary to check out if other seismic observables can emphasize in a better way the effect.

6 Modelling

As it has been shown wave propagation in volcano environments involves many factors that must be taken into account in order to explain the complexity of the wevafield. No so much has been done at high frequencies where supposedly topography, the most important scattering mechanism, seems to play an important role. Cause ADER DG method makes use of tetrahedra element grids, and concerning the meshing process it is computationally much cheaper to implement accurately the geometry with this numerical method compared to others, we consider it is the appropriate method to model our study.

In order to save the amount of elements of the numeral model we must delimit considerably our computational domain to a zone close to the summit, which include just the stations around it. Lets highlight that even working in this reduced volume the high frequencies we pretend to reach (about 30 Hz) make us create tiny elements of 50 m. Our simulations will work with a number of elements about 10 millions and a time computation length of 25 hours (we are interested in the first 10 s of the seismogram).

The a priori strategy to model follows as:

1. Some test simulations without no topography in an homogeneous model need to be done at first in order to ensure that boundary reflections and reflections coming from the coarsening of the mesh (factor that seems to create so much noise) just introduce an acceptable amount of noise in the coda of the synthetic seismograms.

2. The only information that can be accurately modeled on volcano simulations is the topography thanks to the precise digital elevation models available. It seems then to be a logical strategy to evaluate at first what is the influence of this scatter mechanism. We will simulate with different resolutions for the surface, starting from a flat one up to a 100 m resolution one. We point out that though there is no any specific limitation creating more accurate geometries with cubit (it can create even 50 m resolution geometries in a relative short time), for the software in charge of the meshing (simmodeler) it seems still to be computational expensive for being done in serial. Anyway lets also remind that working with dominant frequencies of about 20 Hz, the dominant wavelength will reach values around 200 m so the range of resolution that at the moment we can work with should pay off.

   We highlight as well that simulations with different resolutions for the surface (3000 m, 500 m and 250 m) have already be done up to frequencies of 10 Hz. Some clear differences can be distinguished between seismograms, but affecting mainly to stations which are far from the source and thus not reporting a dramatic change for those ones on the summit. New simulations in a more proper frequency range must be handled in order to clarify the real effect of topography.

Cause we do not know the real source mechanism of the events, we use the simpler, an explosive one, using an explosion avoids effects due to source complexity, for example, the radiaton pattern and finite-fault rupture. The radiation pattern is, therefore, identical in all azimuths, which allows us to focus on the effect of topography alone. With a peak time source function that creates an adequate frequency range. We use a P-wave velocity of 3.8 km/s, velocity suggested from a previous 1D model used for PdF (Florent; Model with a velocity gradient that follow the topography with P wave velocity of 3.5 km/s at the surface and reaching a value of 4.2 km/s al sea level).

3. Layering thin structure: It can be implemented a thin shallow layer which extends just on the summit with different impedance values in order to check out if it is able to modify enough the wavefield.

4. Scattering body: Dimensions and material properties still difficult to infer.

5. Fractal heterogeneity and intrinsic attenuation: This two ingredients can be include in order to make the synthetic seismograms resemble more the real ones, increasing the scattering effect and shortening the seismograms for all the stations, but they should not play an important role to emphasize the behavior of the stations on the summit.

6. 1D velocity model: As it has been mentioned there is available a 1D model already used for Florent.

References

Bachèlery, P., Blum, P., Cheminée, J., Chevallier, L., Gaulon, R., Girardin, N., Jaupart, C., Lalanne, F., Le Mouel, J., Ruegg, J. and Vincent, P. (1982), 'Eruption at the piton de la fournaise volcano on 3 february 1981', *Nature* **297 (5865)**, 395–397.

Battaglia, J. (2001), Seismic quantification of magmatic processes on the Piton de la Fournaise between 1991 and 2000. Thèse d'Université PhD, PhD thesis, University Paris 7, Paris, p.

Battaglia, J., Ferrazzini, V., Staudacher, T., Aki, K. and Cheminée, J.-L. (2005), 'Pre-eruptive migration of earthquakes at the piton de la fournaise volcano (réunion island)', *Geophys. J. Int.* **161**, 549–558.

Bean, C., Lokmer, I. and O'Brien, G. (2008), 'Influence of near near-surface volcanic structure on long-period seismic signals and on momnet tensor inversons: simulated examples from mount etna', *Journal of Geophysical Research* **113 (B8)**, B08308.

Chouet, B. (2003), 'Volcano seismicity', *Pure Appl. Geophys.* **169**, 739–788.

Davi, R., O'Brien, G., Lokmer, I., Bean, C., Lesage, P. and Mora, M. (2010), 'Moment tensor inversion of explosive long period events recorded on arenal volcano, costa rica, constrained by synthetic tests', *Journal of Volcanology and Geothermal Research* **194**, 189–200.

Etienne, V., Chaljub, E., Virieux, J. and Glinsky, N. (2010), 'An hp-adaptive discontinuous galerkin finite-element method for 3-d elastic wave modelling', *Geophys. J. Int.* **183**, 941–962.

Käser, M. and Dumbser, M. (2006), 'An arbitrary high order discontinuous galerkin method for elastic waves on unstructured meshes i: The two-dimensional isotropic case with external source terms', *Geophys. J. Int.* **166**, 855–877.

Käser, M., Dumbser, M., De la Puente, J. and Igel, H. (2007), 'An arbitrary high-order discontinuous galerkin method for elastic waves on unstructured meshes - iii: Viscoelastic attenuation', *Geophys. J. Int.* **168**, 224–242.

Käser, M., Pelties, C., Castro, E. C., Djikpesse, H. and Prange, M. (2010), 'Wave field modeling in exploration seismology using the discontinuous galerkin finite element method on hpc-infrastructure', *The Leading Edge* **29**, 76–85.

Kumagai, H., Chouet, B. and Nakano, M. (2002), 'Waveform inversion of oscillatory signatures in long-period events beneath volcanoes', *Journal of Geophysical Research* **107 (B11)**, 2301.

Lénat, J., Bachèlery, P. and Merle, O. (2012), 'Anatomy of piton de la fournaise volcano (la réunion, indian ocean)', *Bulletin of Volcanology* **74**, 1945–1961.

McNutt, S. (2005), 'Volcanic seismology', *Annu. Rev. Earth Planet. Sci.* **32**, 461–491.

Michon, L., Staudacher, T., Ferrazzini, V., Bachèlery, P. and Marti, J. (2007), 'April 2007 collapse of piton de la fournaise: a new example of caldera formation', *Geophysical Research Letters* **34**, 21.

O'Brien, G., Lokmer, I. and Bean, C. (2010), 'Statistical selection of the best seismic source mechanisms from inversions of synthetic volcanic long-period events', *Journal of Geophysical Research* **115**, B09303.

Ohminato, T., Chouet, B., Dawson, P. and Kedar, S. (1998), 'Waveform inversion of very long period impulsive signals associated with magmatic injection beneath kilauea volcano, hawai', *Journal of Geophysical Research* **103 (B10)**, 23839–23862.

Peltier, A., Bachèlery, P. and Staudacher, T. (2009), 'Magma transport and storage at piton de la fournaise (la réunion) between 1972 and 2007: a review of geophysical and geochemical data', *Journal Volcanology and Geothermal Research* **184(1-2)**, 93–108.

Prôno, E., Battaglia, J., Monteiller, V., J-l, G. and Ferrazzini, V. (2009), 'P-wave velocity structure of piton de la fournaise volcano deduced from seismic data recorded between 1996 and 1999', *Journal Volcanology and Geothermal Research* **184(1-2)**, 49–62.

Ripperger, J., Igel, H. and Wassermann, J. (n.d.), Seismic wave simulation in the presence of real volcano topography, PhD thesis, LMU.

Saccorotti, G., Zuccarello, L., Del Pezzo, E., Ibanez, J. and Gresta, S. (2004), 'Quantitative analysis of the tremor wavefield at etna volcano, italy', *Journal of Volcanology and Geothermal Research* **136(3-4)**, 223–245.

Stieltjes, L. and Moutou, P. (1989), 'A statistical and probablistic study of the historic activity of the piton de la fournaise, reunion island, indian ocean', *Journal of Volcanology and Geothermal Research* **36**, 67–86.

Zecevic, M., De Barros, L., Bean, C., O'Brien, G. and Brenguier, F. (2013), 'Investigating the source characteristics of long-period (lp) seismic events recorded on piton de la fournaise volcano, la reunion', *Journal of Volcanology and Geothermal Research* **258**, 1–11.

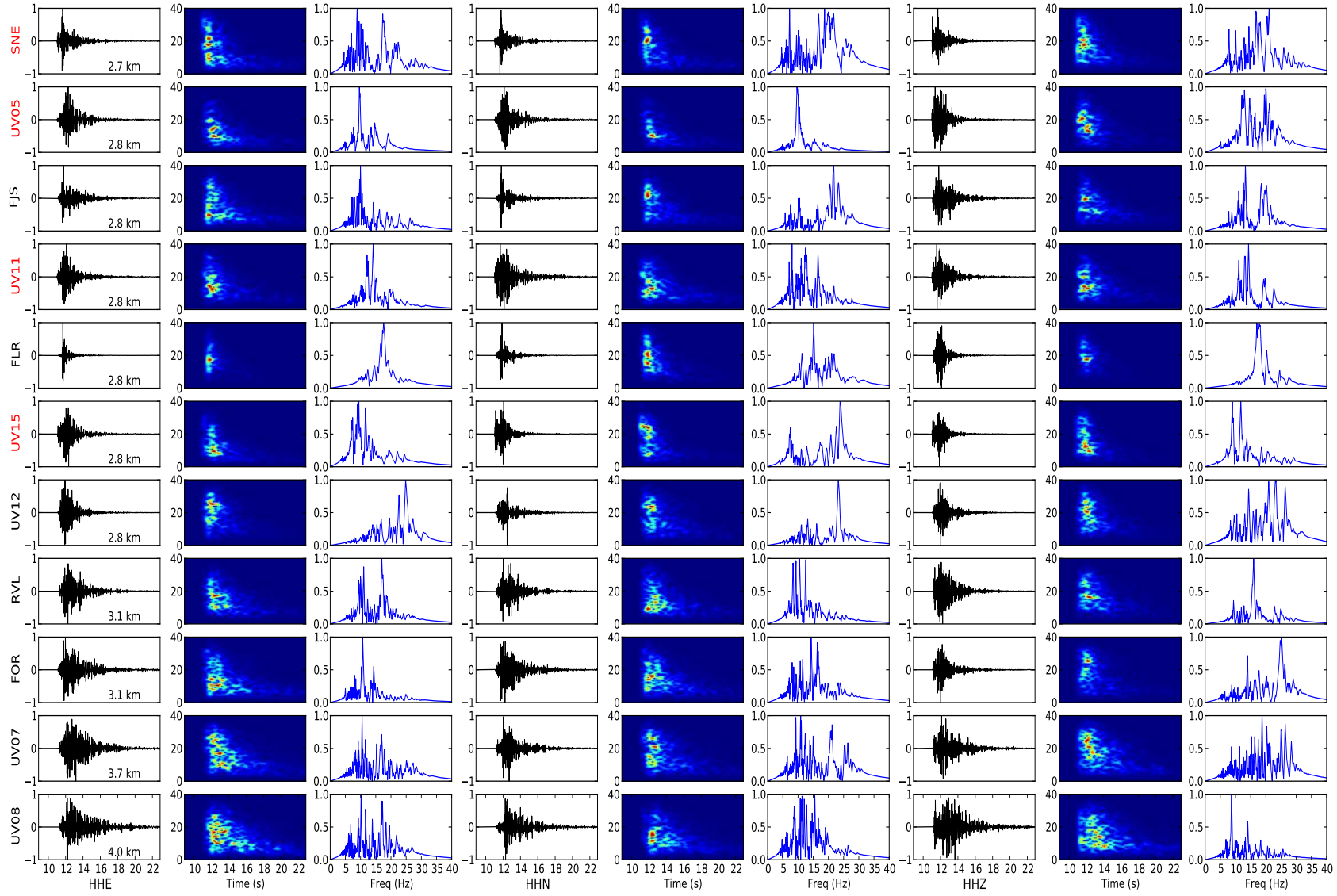

Fig. 16: Eleven three component velocity seismograms (each trace has been normalized by its maximum amplitude), spectrograms and power spectrums of the stations located nearby the summit. The stations are indicated on the left and the component in the bottom of the figure. The distance to the source is indicated on the right of the seismic E component trace. There no exist a clear distintion in the signal among the stations located on the summit (highligthed in red). Conforming distance increases the seismograms seem to exhibit a more distorted waveform.

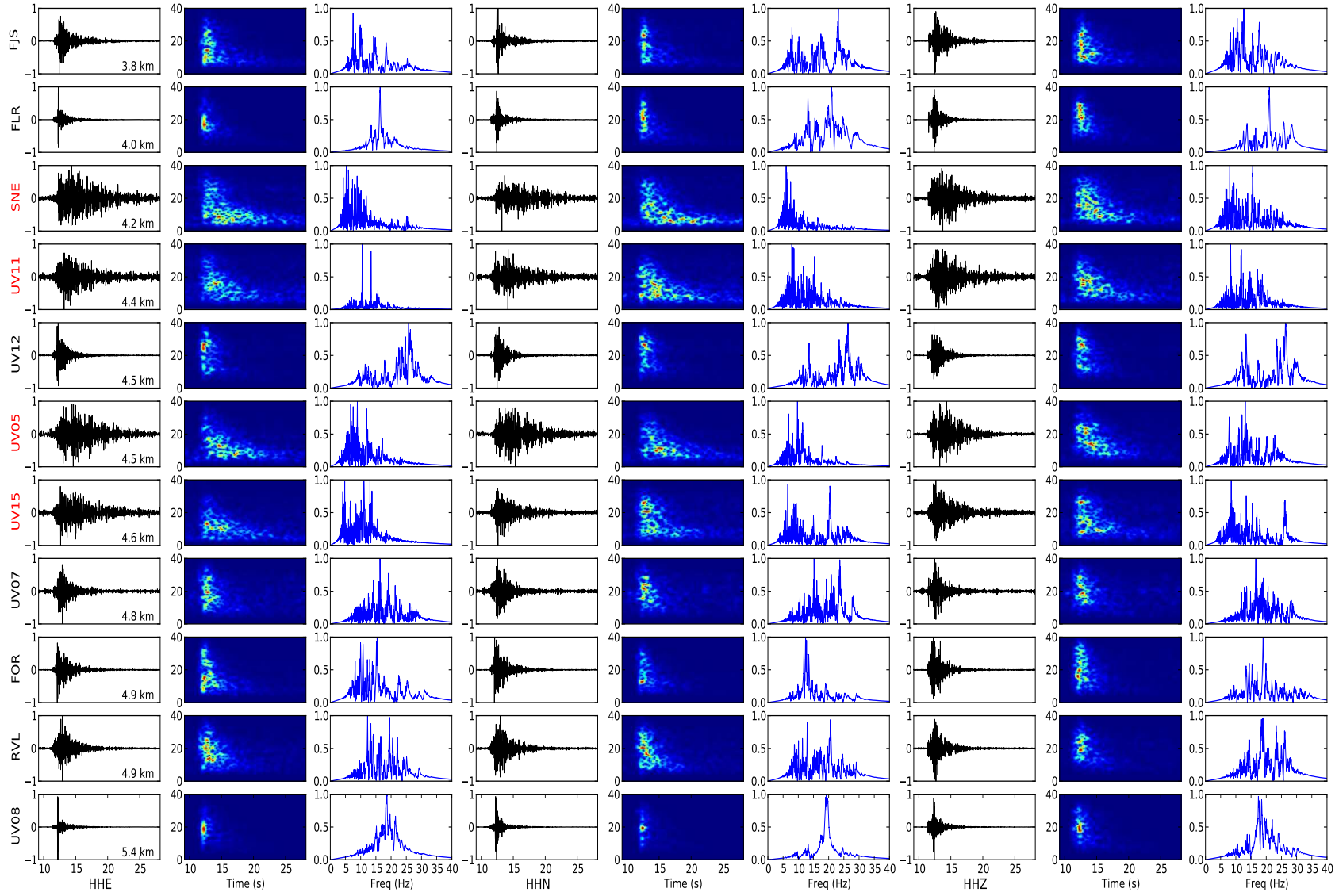

Fig. 17: Three component velocity seismograms, spectrograms and power spectrums of the stations located nearby the summit. The stations are indicated on the left and the component on the bottom of the figure. The distance to the source is indicated on the right of the seismic E component trace. The signal for the stations located close to the crater (highlighted in red) show a very distorted waveform, longer duration and a reduction of the high requencies.